Biomaterials 51 (2015) 161–172

Contents lists available at ScienceDirect

Biomaterials

journal homepage: www.elsevier.com/locate/biomaterials

Doxorubicin-loaded polysaccharide nanoparticles suppress the growth of murine colorectal carcinoma and inhibit the metastasis of murine mammary carcinoma in rodent models

Mingqiang Li [a, d], Zhaohui Tang [a], Dawei Zhang [a], Hai Sun [a], Huaiyu Liu [c], Ying Zhang [a], Yuanyuan Zhang [b, **], Xuesi Chen [a, *]

[a] Key Laboratory of Polymer Ecomaterials, Changchun Institute of Applied Chemistry, Chinese Academy of Sciences, Changchun 130022, PR China
[b] Wake Forest Institute for Regenerative Medicine, Wake Forest School of Medicine, Medical Center Boulevard, Winston-Salem, NC 27157, USA
[c] Laboratory Animal Center, Jilin University, Changchun 130012, PR China
[d] University of Chinese Academy of Sciences, Beijing 100049, PR China

ARTICLE INFO

Article history:
Received 27 August 2014
Received in revised form
30 January 2015
Accepted 1 February 2015
Available online 19 February 2015

Keywords:
Cancer model
Colorectal carcinoma
Mammary carcinoma
Metastasis
Doxorubicin
Chemotherapy

ABSTRACT

As a synergistic drug combination, doxorubicin-loaded cisplatin crosslinked polysaccharide-based nanoparticles (Dex-SA-DOX-CDDP) have demonstrated enhanced antitumor efficacy and reduced systemic toxicity *via* optimized biodistribution, controlled drug release, prolonged blood circulation, and improved tolerability, compared to the non-crosslinked nanoparticles or free doxorubicin. Herein, we apply the Dex-SA-DOX-CDDP nanoparticles as an efficient antitumor agent to treat colorectal and breast tumors in three different *in vivo* models, i.e. subcutaneously implanted colorectal carcinoma, dimethylhydrazine-induced autochthonous colorectal carcinoma, and metastatic mammary carcinoma, which more closely simulate the natural milieu of the original tumor with intact pathological and immunological responses. Based on the properties of this combination in higher tumor accumulation and penetrating efficiency, the Dex-SA-DOX-CDDP nanoparticles significantly decreased the tumor sizes in CT26 cell line xenograft tumors compared to control. In addition, the affected animals' lifespan was significantly extended after the Dex-SA-DOX-CDDP treatment, in the autochthonous colon cancer model. Moreover, with the aid of iRGD, Dex-SA-DOX-CDDP could effectively block primary tumor growth and prevent the metastasis of 4T1 murine mammary carcinoma. In conclusion, Dex-SA-DOX-CDDP nanoparticles remarkably inhibit growth of colorectal carcinoma and metastasis of mammary carcinoma *in vivo*, which provides potential application as a safe and efficient antitumor agent in treatment of these cancers.

1. Introduction

Both colorectal and mammary carcinoma are leading causes of cancer-related mortality worldwide [1–3]. Colorectal carcinoma causes approximately 50,000 deaths in the United States and 655,000 deaths throughout the world per year [4,5]. Breast cancer is the most common malignancy in women, with one in nine women developing breast cancer during their lifetime [6] and cancer death with more than a million newly diagnosed cases annually worldwide [3]. Surgical resection in combination with adjuvant therapy is efficient at the early stages of disease, but subsequent relapse and metastasis often occur. Tumor metastasis is a multistage process in the late stage of the cancers, which is defined as the ability of malignant tumor cells to invade local tissues at the primary site, traverse basement membranes as tissue barriers, migrate and re-establish at distant secondary sites [7]. More than 60% of the malignant tumors have been in progression of metastasis, when they are first diagnosed, while other tumor patients are also subject to tumor metastasis during treatment and even after first recovery for several years [7]. Tumor metastasis is responsible for as much as 90% of cancer-related deaths [8]. Therefore, inhibition of tumor metastasis is critical in cancer

* Corresponding author. Tel./fax: +86 431 85262112.
** Corresponding author.
E-mail addresses: yzhang@wakehealth.edu (Y. Zhang), xschen@ciac.ac.cn (X. Chen).

http://dx.doi.org/10.1016/j.biomaterials.2015.02.002
0142-9612/

therapy. Although significant progress has been made in the development of anticancer therapies, reduced toxicity and increased treatment efficiency of antimetastasis drugs are still much in demand.

Nanoparticle-mediated delivery of chemotherapeutic agents has demonstrated enhanced anticancer efficacy and reduced systemic toxicity in cancer treatment [9,10]. Nanomedicines with the proper sizes and surface properties provide a controlled release of anticancer drug system to retain optimal levels of drugs within solid tumors when injected into target tissues. In addition, this system may avoid the drugs rush into blood circulation, and enhances permeability and retention (EPR) effect of drugs in the host when systematically administrated [11]. Before EPR-based drug targeting technic can be translated to the clinic, a number of these therapeutics with nanotechnology (nanomedicines) for cancer treatment have been tested in animal experiments with promising results. Some are under clinical trials and some have been approved by the United States Food and Drug Administration (FDA) and other international equivalents for clinical use [11,12]. In particular, the success of polymeric micelles including Oncaspar (approved by FDA for acute lymphoblastic leukemia in 2006), Genexol-PM (approved by South-Korea for metastatic breast cancer in 2006), NK 911 (in phase II for pancreatic and colorectal cancers in Japan), NK 105 (in phase II for stomach cancer in Japan) and NK 012 (in phase II for breast cancer in Japan and USA) brings hope to the polymer-based nanomedicines for cancer therapy [13,14].

Animal models have been used as the front line in predicting efficacy and finding toxicities for cancer chemotherapeutic agents before entering the clinic [15]. Currently, the most common animal models used for the development of potential antitumor agents involve subcutaneous implantation of cultured murine tumor cell lines into syngenic mouse strains or injection of human tumor cell lines into immunocompromised mice [16,17]. Subcutaneous tumor models are widely used because of their simplicity. In addition, the primary tumor growth can be conveniently monitored by periodic caliper measurements to evaluate the therapeutic efficacy. Nevertheless, the ectopic subcutaneous models possess limited pathophysiological relevance, heterogeneity and clinical predictability[18,19]. Compared to the ectopic subcutaneous tumor-implantation model, carcinogen-induced models more closely simulate the natural milieu of the original tumor, with intact pathological and immunological responses. Especially, carcinogen-induced models can effectively recapitulate the time-dependent and multistage progression of tumor pathogenesis in response to environmental carcinogens and tumor-promoting agents [17]. Their molecular, biochemical, and histopathological characteristics are similar to the developmental consequences of specific human cancers, from hyperplasias, pre-malignant lesions, low grade well-differentiated carcinomas, and ultimately to invasive and more poorly differentiated carcinomas [20,21]. Consequently, carcinogen-induced primary tumor models have been used as a general class of preclinical cancer models to offer various distinct advantages and clinical relevance to human cancers. Orthotopic tumor models more closely mimic the human clinical course of metastatic disease. Generally, they involve the implantation of cultured tumor cells or primary tumor tissue explants into the originating tissue site of the cancer in rodents, resulting in much higher metastatic rates and a pathological phenotype [17,22]. Multiple preclinical models of cancers are indispensable in the drug discovery and development process for new cancer drugs. Moreover, evaluating the efficacy of novel therapeutic agents in a variety of preclinical models can better mimic the heterogeneity of human cancers and also assist in establishing dose levels, dose regimens and drug combinations for use in clinical trials [17]. At present, the therapeutic effects of most of the reported nanomedicines have been just evaluated in one subcutaneous tumor model with lack of continuous and intensive investigations.

We have demonstrated that, by favored biochemical property of cisplatin (CDDP) pro-drug as the cross-linker for doxorubicin (DOX) delivery, the rationally-designed polysaccharide-based drug delivery system (doxorubicin-loaded cisplatin crosslinked dextran-based nanoparticles, Dex-SA-DOX-CDDP, Scheme 1A) facilitated intracellular drug delivery and inhibited tumor growth in A549 xenograft murine model [23]. In addition, antitumor drug loading procedure can be efficiently performed in aqueous medium with non-toxic reagents or organic solvents, thus representing a safe approach with green chemistry action. Importantly, *in situ* crosslinking of the DOX-loaded polysaccharide nanoparticles by introducing a small amount of cisplatin as the crosslinker significantly increase the surface charge and stability. This would further improve the tolerability, *in vivo* pharmacokinetics, bio-distribution, and antitumor efficacy, and reduce drug-related multiorgan toxicity side-effect. Despite the great potential of Dex-SA-DOX-CDDP nanoparticles for cancer therapy, the detailed application and more comprehensive study of such nanoparticle system for other solid tumor models, especially for orthotopic and metastatic models, have not been explored.

In the present study, for the first time, we aim to evaluate the therapeutic efficacy of Dex-SA-DOX-CDDP nanoparticles in three solid tumor animal models, including subcutaneous colorectal carcinoma, primary colorectal carcinoma and metastatic mammary carcinoma. With the reinforced stability, prolonged blood circulation and efficient delivery of drug into the tumor tissues, we propose that Dex-SA-DOX-CDDP can efficiently suppress the growth of murine colorectal carcinoma. Furthermore, it has been reported that co-administration of nanomedicines with internalizing arginine–glycine–aspartic acid (iRGD), a tumor specific vascular-extravasation and tissue-penetration peptide that combines RGD with a tumor-penetrating CendR motif (RGDK/R), exhibits enhanced tumor targeting, penetration, and therapeutic effect compared to the single nanomedicines [24–27]. Currently, clinical trials are under way in the United States to evaluate the effect of iRGD on tumor vasculature [28]. In this study, we also demonstrate for the first time that co-administration of iRGD and Dex-SA-DOX-CDDP may not only effectively block primary tumor growth, but also prevent the metastasis of murine mammary carcinoma (Scheme. 1B), which is significantly important for the development of new approaches to metastatic cancer treatment. We believe that the therapeutic evaluation of Dex-SA-DOX-CDDP nanomedicine in these specific types of preclinical tumor models is crucial and necessary for its further development in clinical applications.

2. Materials and methods

2.1. Materials

Dex-SA-DOX-CDDP nanoparticles were synthesized according to the previous report [23]. 3-(4,5-Dimethyl-thiazol-2-yl)-2,5-diphenyl tetrazolium bromide (MTT, Sigma), 4′,6-diamidino-2-phenylindole dihydrochloride (DAPI, Sigma), ethylenediaminetetraacetic acid disodium salt (EDTA-Na_2, Tianjin Guangfu Fine Chemical Research Institute, China) and dimethylhydrazine (DMH, TCI, Tokyo, Japan) were used without further purification. Cyclic iRGD (CRGDKGPDC) was customized from Apeptide Co. Ltd. (Shanghai, China). All other reagents and solvents were of analytical grade and used without further purification.

2.2. Animals

Male or female Balb/c mice at 5–6 weeks of age were obtained from Beijing HFK Bioscience Co., Ltd. All animals received care in compliance with the guidelines outlined in the Guide for the Care and Use of Laboratory Animals and all procedures were approved by the Animal Care and Use Committee of Jilin University.

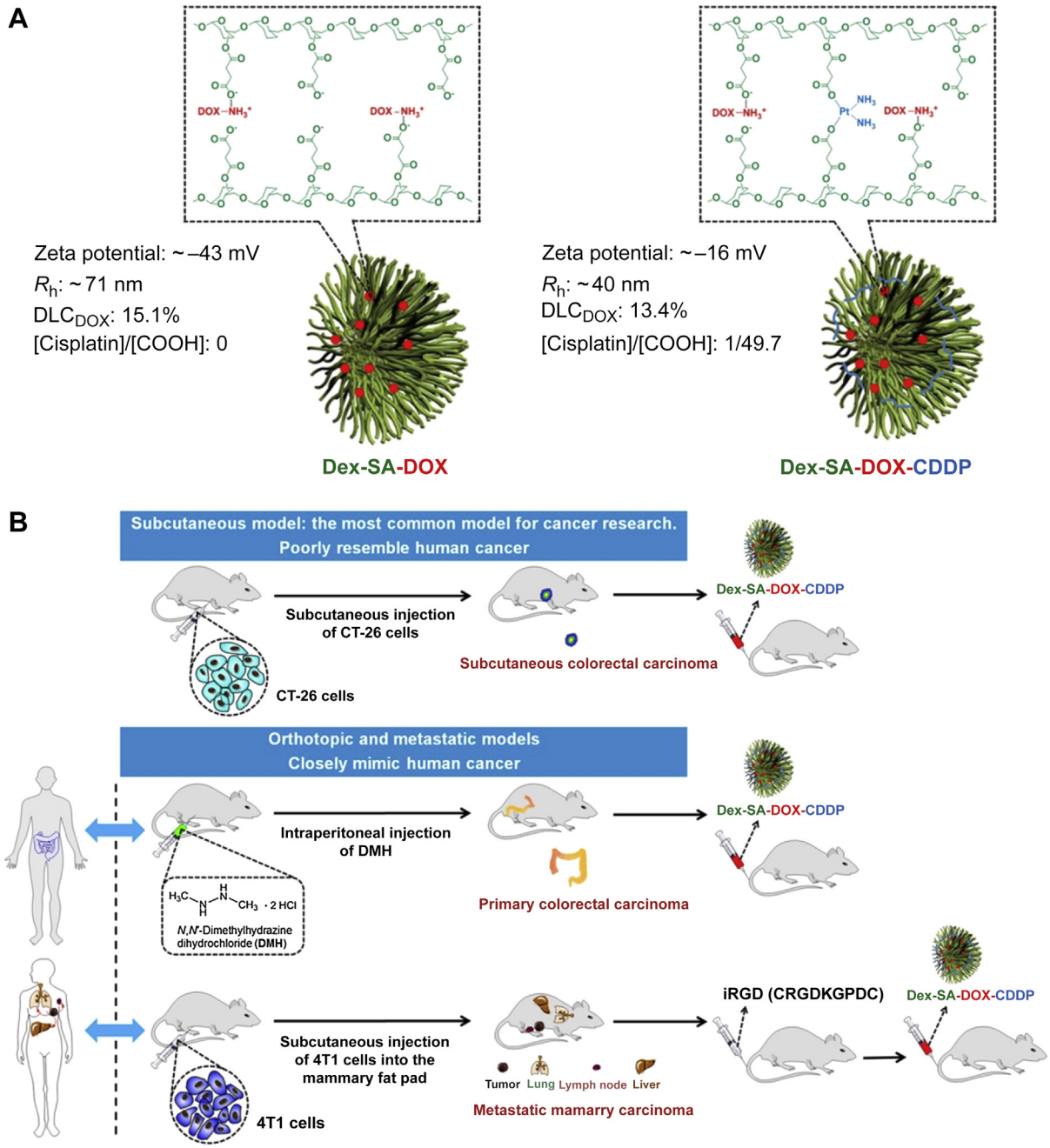

Scheme 1. (A) Schematic illustration of the chemical composition and process of preparing Dex-SA-DOX-CDDP. The Dex-SA-DOX-CDDP condenses into nanoparticles with a mean diameter around 80 nm. (B) Schematic illustration of preparing subcutaneous colorectal carcinoma, primary colorectal carcinoma, and metastatic mammary carcinoma models and their corresponding treatment programs.

2.3. Cell lines and cell culture

Cell lines CT26 (murine colon carcinoma) and 4T1 (murine mammary carcinoma) were obtained from the Cell Bank of the Chinese Academy of Sciences (Shanghai, China). The CT26 cells were cultured at 37 °C in a 5% CO_2 atmosphere in Dulbecco's modified Eagle's medium (DMEM, Gibco) supplemented with 10% fetal bovine serum (FBS, heat-inactivated, Kang Yuan Biology, Tianjin, China), penicillin (50 U mL^{-1}) and streptomycin (50 U mL^{-1}). The 4T1 cells were cultured in RPMI medium 1640 (Gibco) supplemented with 10% FBS (heat-inactivated, Hyclone), penicillin (50 U mL^{-1}), streptomycin (50 U mL^{-1}), glucose (2.5 g L^{-1}) and sodium pyruvate (0.11 g L^{-1}) at 37 °C in a humid atmosphere with 5% CO_2. The cell density was determined before each experiment using a hemocytometer.

2.4. Cytotoxicity assay

The cytotoxicities of Dex-SA, free DOX plus free CDDP, Dex-SA-DOX plus Dex-SA-CDDP and Dex-SA-DOX-CDDP were evaluated by MTT assay. The CT26 or 4T1 cells were seeded in 96-well plates (8×10^3 cells per well) in 100 μL of culture medium and incubated at 37 °C in a 5% CO_2 atmosphere for 24 h. The culture medium was replaced with 200 μL of fresh medium containing Dex-SA, free DOX plus free CDDP, Dex-SA-DOX plus Dex-SA-CDDP and Dex-SA-DOX-CDDP. The cells were subjected to MTT assay after being incubated for another 24 or 48 h. The absorbency of the solution was measured on a Bio-Rad 680 microplate reader at 490 nm. The relative cell viability was determined by comparing the absorbance at 490 nm with control wells containing only cell culture medium. Data are presented as means ± standard deviation ($n = 6$).

2.5. Drug distribution within CT26 tumor tissues

The distributions of DOX in tumor tissues were analyzed by confocal laser scanning microscopy (CLSM). Briefly, a mouse colorectal carcinoma model was generated by subcutaneous injection of CT26 cells (1.5×10^6) in the right flank of each mouse (male Balb/c mice, 5–6 weeks old). When the tumor volumes reached

200–300 mm^3, the mice were administered intravenously with free DOX, Dex-SA-DOX and Dex-SA-DOX-CDDP at an equivalent DOX dose of 5 mg kg^{-1}. The mice were sacrificed at 3, 10, and 24 h post-injection, and the tumor tissues were collected, fixed in tissue freezing medium, sectioned (5 μm thick) and counterstained with DAPI for the cell nucleus. The coverslips were mounted on glass microscope slides with a drop of glycerin and sealed with nail polish to prevent drying and movement under microscope. The cellular localization was visualized under a laser scanning confocal microscope (Carl Zeiss, LSM 780). The average signal intensities of DOX were quantitatively analyzed using the commercial software (ZEN black 2011).

2.6. In vivo antitumor evaluation with subcutaneous colorectal carcinoma model

A mouse colorectal carcinoma model was generated by subcutaneous injection of CT26 cells (1.5×10^6) in the right flank of each mouse as described above. When the tumor volumes reached approximately 100 mm^3, the mice were randomly divided into five groups and treated with PBS, Dex-SA (30.0 mg kg^{-1}), free DOX (4.0 mg kg^{-1}) plus free CDDP (0.43 mg kg^{-1}), Dex-SA-DOX (4.0 mg kg^{-1} on DOX basis) plus Dex-SA-CDDP (0.43 mg kg^{-1} on cisplatin basis) and Dex-SA-DOX-CDDP (4.0 mg kg^{-1} on DOX basis and 0.43 mg kg^{-1} on cisplatin basis) by intravenous injection on days 0, 4 and 8. The treatment efficacy and systemic toxicity were assessed by measuring the tumor volume and body weight, respectively. The tumor volume and tumor inhibition rate were calculated by the following formula [29,30]:

$$\text{Tumor volume } (V) = a \times b^2/2$$

$$\text{Tumor inhibition rate (TIR, \%)} = [(W_c - W_x)/W_c)] \times 100\%$$

a and b were the longest and shortest diameter of the tumors measured by vernier caliper. W_c represented the average weight of tumors in control group, while W_x represented the average weight of tumors in treatment group.

2.7. Tumor suppression study in autochthonous colorectal carcinoma model

The primary colorectal carcinoma model was established according to the previous protocol with minor modification [31,32]. Briefly, DMH was dissolved in 0.001 M EDTA-Na_2, and then its pH was adjusted to 6.5 with a few drops of 0.01 M NaOH. Male Balb/c mice (5–6 weeks old) were intraperitoneally injected with DMH (30 mg kg^{-1} body weight) twice a week for 16 weeks to induce colon tumors. After the last injection of DMH, the mice were randomly divided into five groups, and treated with PBS, Dex-SA (30.0 mg kg^{-1}), free DOX (4.0 mg kg^{-1}) plus free CDDP (0.43 mg kg^{-1}), Dex-SA-DOX (4.0 mg kg^{-1} on DOX basis) plus Dex-SA-CDDP (0.43 mg kg^{-1} on cisplatin basis) and Dex-SA-DOX-CDDP (4.0 mg kg^{-1} on DOX basis and 0.43 mg kg^{-1} on cisplatin basis) by intravenous injection every week for a total of five cycles (at weeks 16–20). All mice that survived at end of the experiment were terminated at the 34th week.

2.8. In vivo antitumor effects in metastatic mammary carcinoma model

The metastatic mammary carcinoma model was generated by the subcutaneous injection of 4T1 cells (1.5×10^6) into the mammary fat pad of the mice (female Balb/c mice, 5–6 weeks old). When the tumor volumes reached approximately 50 mm^3, the mice were randomly divided into seven groups and then treated with PBS, Dex-SA (3.0 mg kg^{-1}), iRGD (4.0 mg kg^{-1}), free DOX (3.0 mg kg^{-1}) plus free CDDP (0.32 mg kg^{-1}), iRGD plus free DOX (3.0 mg kg^{-1}) plus free CDDP (0.32 mg kg^{-1}), Dex-SA-DOX-CDDP (3.0 mg kg^{-1} on DOX basis and 0.32 mg kg^{-1} on cisplatin basis) and iRGD plus Dex-SA-DOX-CDDP (3.0 mg kg^{-1} on DOX basis and 0.32 mg kg^{-1} on cisplatin basis) by intravenous injection on days 0, 4, 8 and 12. In the iRGD co-administration groups, iRGD was injected 1 h before the treatment of chemotherapeutic agents. The treatment efficacy and systemic toxicity were assessed by measuring the tumor volume and body weight, respectively. The tumor volume and tumor inhibition rate were calculated as described above.

2.9. Histological and immunohistochemical analyses

For the subcutaneous colorectal carcinoma model and metastatic mammary carcinoma model, the mice were sacrificed at day 16 and 20, respectively. The tumors and major organs (heart, liver, spleen, lung, kidney and lymph node) were collected immediately, fixed in 4% PBS buffered paraformaldehyde overnight, and then embedded in paraffin. The paraffin-embedded tumors and organs were cut at 5 μm thickness, and stained with hematoxylin and eosin (H&E) to assess histological alterations by microscope (Olympus CX31; objective lens: 20×). Immunohistochemistry was performed as described previously [23,33]. Rabbit monoclonal primary antibody for cleaved PARP1 (Abcam, Cambridge, MA, USA) and PV-6000 two-step immunohistochemistry kit (polymer detection system for immuno-histological staining; Zhongshan Goldbridge Biotechnology, Beijing, China) were used in this study.

For autochthonous colorectal carcinoma model, the mice were sacrificed for humane reasons at the end of the experiment. The colon tissue was immediately excised, fixed in 4% PBS buffered paraformaldehyde and embedded in paraffin for H&E staining.

2.10. Statistical analysis

All experiments were performed at least three times and expressed as means ± standard deviation. Data were analyzed for statistical significance using Student's test. $p < 0.05$ was considered statistically significant, and $p < 0.01$ was considered highly significant.

3. Results and discussion

3.1. In vitro cytotoxicity

Our previous study demonstrated that carboxylic ligand functionalized dextran (dextran–succinic acid, Dex-SA) efficiently adsorbed doxorubicin hydrochloride electrostatically in aqueous solution and self-assembled into polymeric micelles (Dex-SA-DOX, non-crosslinked nanoparticles, NCL-Nanoparticles) with uniform size [23]. Subsequently, the crosslinked nanoparticles (CL-Nanoparticles, Dex-SA-DOX-CDDP) were synthesized *in situ* by crosslinking the micelles *via* chelate interactions between the ionic polymeric carrier and the platinum (II) antitumor drug (Scheme 1A).

In vitro cytotoxicity was a crucial issue that needed to be addressed before the drug delivery vector was utilized for *in vivo* tumor chemotherapy. In the current study, the biocompatibility studies using CT26 and 4T1 cells revealed that Dex-SA carrier was nontoxic up to the highest testing concentration of 1 g L^{-1} (Fig. S1), indicating its excellent biocompatibility. As shown in Fig. 1, all the drug formulations demonstrated dose and time dependent toxicity toward CT26 and 4T1 cells. At an equivalent drug concentration, Dex-SA-DOX plus Dex-SA-CDDP revealed a slightly lower cell killing efficiency as compared to free DOX plus free CDDP, whereas the Dex-SA-DOX-CDDP nanoparticles induced the lowest cancer cell killing potency. But this gap was narrowed when the incubation time was extended to 48 h, especially at the high drug concentrations. It was due to free drug that could easily cross the cell membrane, while the DOX-loaded nanoparticles had to be internalized *via* endocytosis. In addition, the drug release from the CL-Nanoparticles was accelerated within the acidic intracellular endosome/lysosome, thus resulting in the lower *in vitro* cytotoxic efficiency [23]. However, for *in vivo* applications, it is unlikely that such a high concentration of free drugs would be present for such a long treatment time [34]. The *in vitro* results also suggested that the Dex-SA-DOX-CDDP nanoparticles with reinforced stability and prolonged blood circulation might facilitate its passive accumulation at tumor tissue *via* EPR effect [35].

3.2. Tumor accumulation and in vivo antitumor effect in subcutaneous colorectal carcinoma model

The prolonged circulation time in blood facilitated the accumulation of Dex-SA-DOX-CDDP in tumors *via* the EPR effect [36]. To further test the accumulation and penetration of drugs in the solid tumor interior, Balb/c mice bearing CT26 tumors were injected with DOX, Dex-SA-DOX and Dex-SA-DOX-CDDP at equivalent dose of doxorubicin (5 mg kg^{-1}). After different time intervals, the tumors were excised, sectioned, stained with DAPI and observed under a confocal microscopy for the detailed distribution of DOX in tumor (Fig. 2A). As shown in Fig. 2B (See the amplificatory images in the Supplementary Data, Figs. S2–S4), both Dex-SA-DOX and Dex-SA-DOX-CDDP accumulated at higher levels than free DOX in the tumor tissue at all the time points. Moreover, compared to the NCL-Nanoparticles, the CL-Nanoparticles displayed much stronger red fluorescence of DOX in the tumor tissue section. These results support the assertion that the slightly negative charged surface and enhanced micellar stability of DOX-loaded Dex-SA micelles after cisplatin crosslinking appeared to be particularly significant for

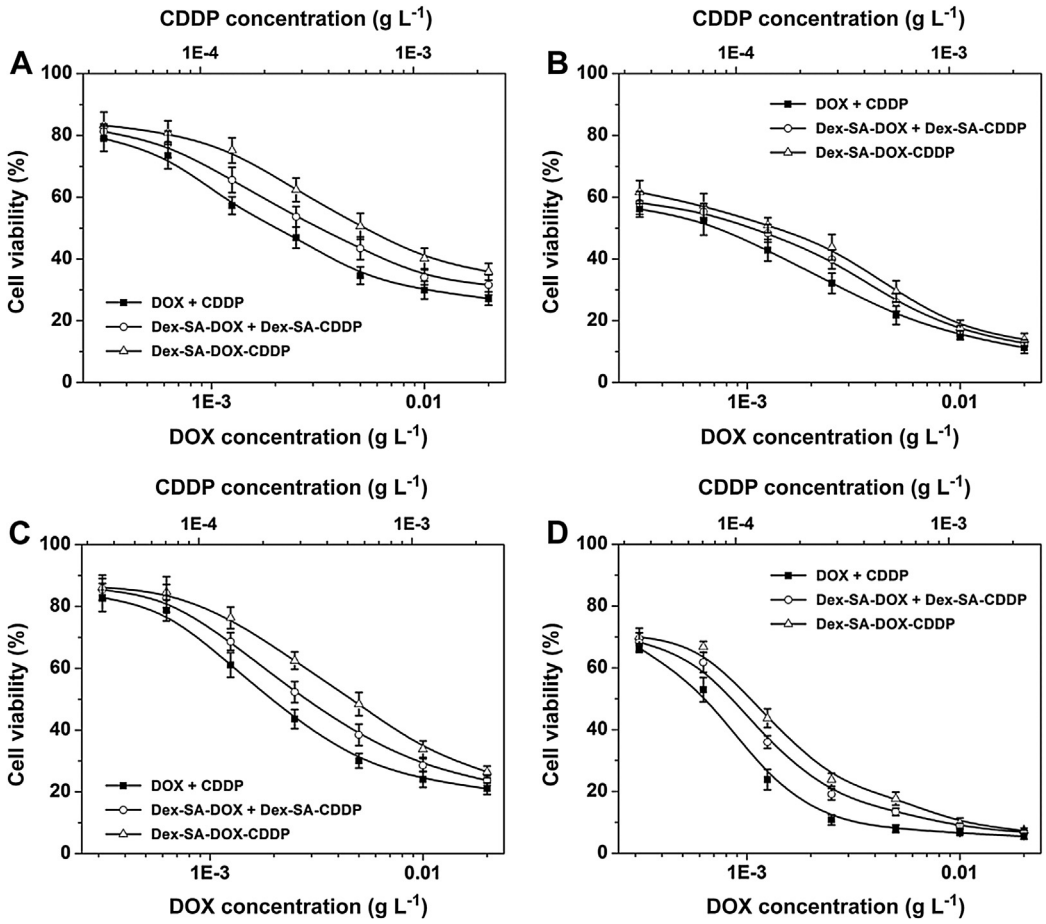

Fig. 1. (A and B) *In vitro* cytotoxicities of DOX plus CDDP, Dex-SA-DOX plus Dex-SA-CDDP and Dex-SA-DOX-CDDP to CT26 cells after incubation for 24 and 48 h. (C and D) Cytotoxicities of the three different formulations to 4T1 cells after incubation for 24 and 48 h.

blood circulation and tumor accumulation. The semi-quantitative mean fluorescence intensity analysis of the tumor tissues also indicated that the uptake of Dex-SA-DOX-CDDP by the tumor cells was much higher than the uptake of DOX and Dex-SA-DOX (Fig. 2C), which was consistent with the imaging data. The mean fluorescence intensity of DOX and Dex-SA-DOX in the tumor tissues did not increase significantly over time, however, the fluorescence signal of Dex-SA-DOX-CDDP continuously increased during the 24 h experimental period. At 24 h, the mean fluorescence intensity of Dex-SA-DOX-CDDP was 2.3 and 1.5-fold higher than those of DOX and Dex-SA-DOX groups, respectively. The increased penetration and accumulation of Dex-SA-DOX-CDDP in tumor might be attributed to the suitable particle size and slightly negatively charged surface, which were beneficial for the reduced nonspecific binding, prolonged circulation time, and finally facilitated the accumulation in tumor *via* the EPR effect [37–39]. All these results confirmed that the Dex-SA-DOX-CDDP nanoparticles showed higher tumor accumulation and penetrating efficiency, which could contribute to increase the cancer therapy efficiency.

Inspired by the prolonged circulation and enhanced tumor localization, we then explored if the Dex-SA-DOX-CDDP could be used as the efficient antitumor agent without unexpected side effects. To provide *in vivo* evidence for the antitumor potential of Dex-SA-DOX-CDDP, the antitumor efficacy was first investigated on Balb/c mice bearing subcutaneous CT26 tumors. As shown in Fig. 3A, compared with the control group (treatment with PBS), the tumor growth was effectively inhibited in all the groups treated with DOX-loaded formulations ($^{***}p < 0.001$), whereas the tumor volumes of mice treated with PBS and blank Dex-SA were similar, indicating that the polymeric drug carrier had no effect on tumor growth. As compared to DOX plus CDDP and Dex-SA-DOX plus Dex-SA-CDDP groups, intravenous injection of Dex-SA-DOX-CDDP was more efficient in inhibiting tumor growth, indicating that the cisplatin prodrug crosslinked structure was critical for tumor suppression. The enhanced tumor inhibition of Dex-SA-DOX-CDDP might be explained by the enhanced accumulation of the CL-Nanoparticles at the tumor site. Furthermore, the effective encapsulation of DOX against leakage in the bloodstream and the facilitated intracellular release of DOX might also contribute to the observed enhanced antitumor efficacy [23,40]. In addition, compared with the free drugs treatment group (DOX plus CDDP), which exhibited an obvious weight loss (10.1% body weight loss; $^{***}p < 0.001$, compared with all the other groups), Dex-SA-DOX-CDDP treatment resulted in almost no difference in body weight after 16 days (Fig. 3B). Such differences demonstrated that the encapsulation of DOX in the reversible CL-Nanoparticles reduced the random exposure of drug to normal tissues, increased the passive accumulation efficacy of the nanoparticles to the tumor sites, and thus led to lower undesirable systemic toxicities and enhanced antitumor efficacy [23]. However, for the PBS control and Dex-SA groups, the sustained increase of body weight (approximately 10.7 and 10.1% body weight gain at day 16) could be explained by the continuous tumor growth. At the end of the experiment, the tumors were dissected from mice and weighted. The mass of the tumors was in the following order: PBS ≈ Dex-SA > DOX plus CDDP > Dex-SA-DOX plus Dex-SA-CDDP > Dex-SA-

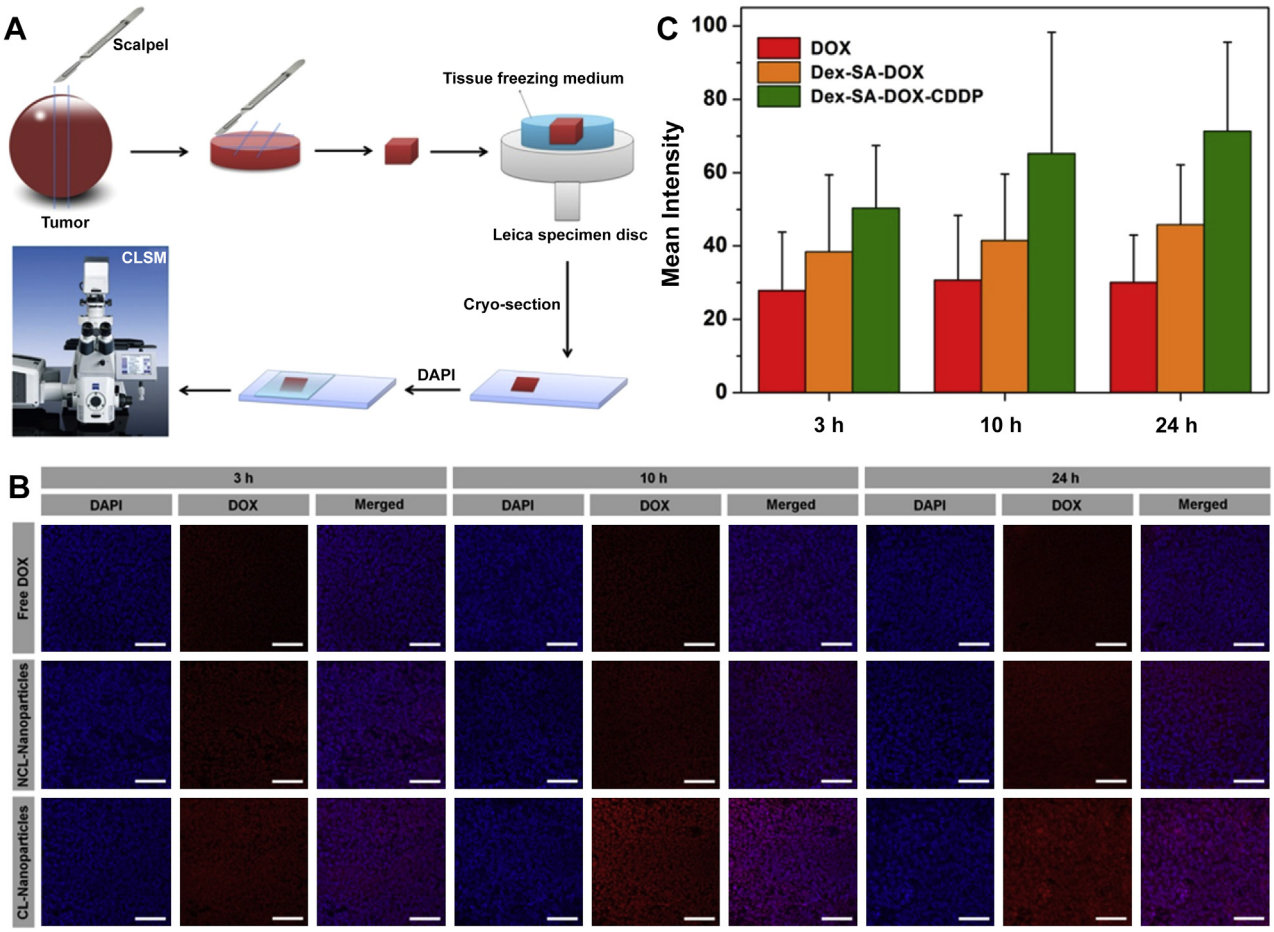

Fig. 2. (A) The schematic illustration of the process of preparing tumor frozen sections. (B) Representative fluorescence micrographs of tumor frozen sections at 3, 10 and 24 h after injection of DOX, Dex-SA-DOX and Dex-SA-DOX-CDDP. Blue fluorescence shows nuclear staining with DAPI and red fluorescence shows the location of DOX. The scale bars represent 100 μm. See the amplificatory images in the Supplementary Data. (C) Mean fluorescence intensity of DOX in the tumor sections treated with DOX, Dex-SA-DOX and Dex-SA-DOX-CDDP. Data were collected from CLSM analyses (ZEN black 2011 software). (For interpretation of the references to colour in this figure legend, the reader is referred to the web version of this article.)

DOX-CDDP, which agreed well with the tumor volumes (Fig. 3C). Correspondently, Dex-SA-DOX-CDDP exhibited the highest inhibition rate (Fig. 3D).

To further evaluate therapeutic efficacy after treatment with various formulations, the tumors were dissected from mice and sectioned for pathology analysis, after 16 days. As shown in Fig. 4A, the tightly packed tumor cells interspersed with large amount of stroma were observed in the tumor tissue treated with PBS and Dex-SA groups, in which more chromatin and binucleolates were also observed, indicating a rapid tumor growth [41]. After the treatment with chemotherapeutic agents, the histological features of tumors exhibited significant differences from the control group. The tumor cellularity decreased significantly and various degrees of tissue necrosis, extensive nuclear shrinkage and fragmentation were observed in the DOX-loaded formulations treated groups. Particularly, the necrosis area in the Dex-SA-DOX-CDDP group was the largest among the tested groups, indicating more efficiency on prevention of cancer cell expansion. This was also consistent with the *in vivo* antitumor capability that the Dex-SA-DOX-CDDP nanoparticles exhibited the highest antitumor efficacy. The immunohistochemistry analysis of the tumor sections was further conducted to detect the expression of cleaved 25 kDa fragment of PARP1 (c-PARP1), one of the essential substrates cleaved by both caspase-3 and -7 and a characteristic hallmark of apoptosis [23,42]. More intensive positive signals were detected in the Dex-SA-DOX-CDDP treated tumors compared with DOX plus CDDP and Dex-SA-DOX plus Dex-SA-CDDP treated ones, indicating that more cells underwent apoptosis in the CL-Nanoparticles treated group. All these results demonstrated that Dex-SA-DOX-CDDP could efficiently deliver DOX to the tumor site, leading to reduced cell proliferation and increased apoptosis *in vivo*, which resulted in a persistent inhibition of tumor growth.

In addition, the representative sections of the main organs including heart, liver, spleen, lung, and kidney taken at day 16 from the control mice receiving PBS and the mice receiving various drug formulations were stained by H&E (Fig. 4B). Histological analysis of the fixed tissues showed that no significant signals of organ damage, inflammatory response, degeneration, and necrosis could be detected in spleen and lung derived from animals in the control group compared to mice treated with Dex-SA, DOX plus CDDP, Dex-SA-DOX plus Dex-SA-CDDP and Dex-SA-DOX-CDDP. Nevertheless, varying degrees of heart, and liver damages were observed from H&E stained organ slices in all the DOX involved groups. Obvious cardiotoxicity was induced by DOX plus CDDP treated groups due to the observed hyperemia, myocardial fiber breakage with acute inflammatory cell infiltration, critical pathological changes, and necrosis of the muscle fibers in cardiac tissue, which was in consistent with the previous report [43]. In contrast, the treatment of tumor bearing mice by DOX-encapsulated CL-Nanoparticles obviously reduced the blight of heart. This was in accordance with

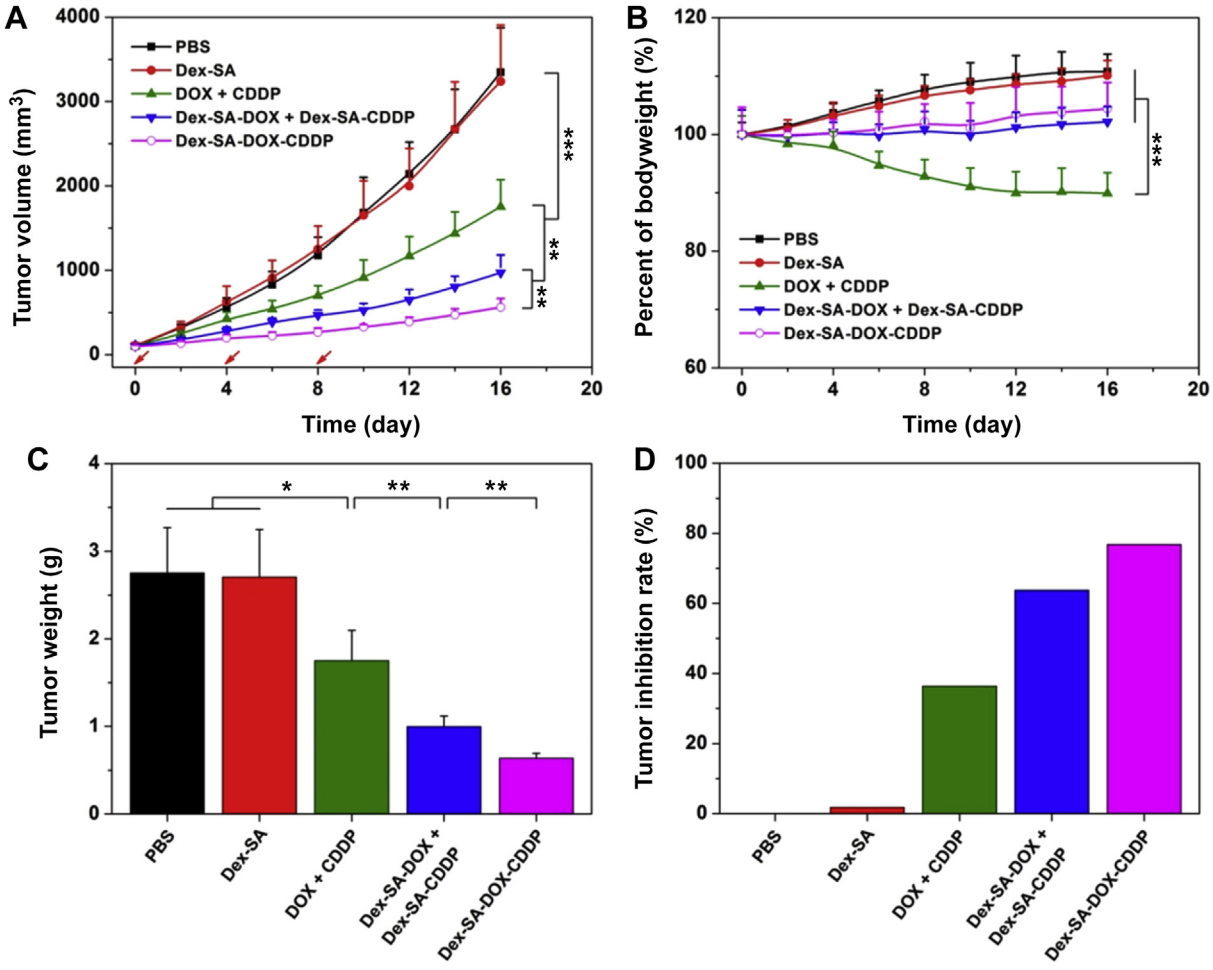

Fig. 3. *In vivo* antitumor efficacy of different formulations against CT26 xenograft tumors (subcutaneous colorectal carcinoma). Data were presented as means ± standard deviation ($n = 6$). (A) Tumor sizes of the mice as a function of time. The arrows represented the day on which the intravenous tail vein injection was performed. The Dex-SA-DOX-CDDP group demonstrated significant tumor inhibition (***$p < 0.001$, compared to control and Dex-SA groups; **$p < 0.01$, compared to DOX plus CDDP and Dex-SA-DOX plus Dex-SA-CDDP groups). (B) Body weight changes with the time of tumor-bearing mice. The mice administrated Dex-SA-DOX-CDDP nanoparticles maintain the body weight (***$p < 0.001$, compared to DOX plus CDDP group). (C) Tumor weight at the end of the experiment. (D) Tumor inhibition rate of mice after 16-day treatment.

our previous biodistribution study, in which the accumulation of Dex-SA-DOX-CDDP in heart was found relatively lower than free DOX [23]. On the other hand, the delayed drug release of DOX from the carriers during the blood circulation might also contribute to the decreased cardiotoxicity. Slight structural disturbance with microregional necrosis of hepatocytes could be observed in the liver for all the chemotherapeutic drugs treated groups. However, after the *in situ* crosslinking by CDDP, the side effects were distinctly inhibited. Besides, the fast liver regeneration with healthy hepatocytes could help the animals for effective recovery from the metabolic break [44]. In agreement with our previous results, free CDDP at a low dose could also induce severe nephrotoxicity (*e.g.*, marked necrosis in proximal tubules, thickening of the mesangium and glomerular basement membrane, and contraction of epithelial luminal space). Nevertheless, the nephrotoxicity of CDDP could be significantly inhibited after chelation with the polymeric carrier. All these results indicated that Dex-SA-DOX-CDDP presented high biocompatibility and showed more promising for further clinical applications.

3.3. Antitumor effect in autochthonous colon cancer model

Taking the advantages of Dex-SA-DOX-CDDP in terms of the high antitumor effect and the excellent biocompatibility, we then further test its therapeutic efficacy in autochthonous tumor model. In autochthonous models, the interactions between tumor cells and their microenvironment are more representative of specific tumor histotypes than transplanted xenografts because of their *in situ* and autochthonous origin [45,46]. Here, a DMH-induced autochthonouscolon cancer model, which was known to closely mimic human colorectal tumor in terms of disease presentation and gross and microscopic pathology [32,47], was chosen to evaluate the antitumor capability of Dex-SA-DOX-CDDP nanoparticles (Scheme. 1B). The mouse colon tumors were first induced by intraperitoneal (i.p.) injection of DMH twice a week for 16 weeks. They were then intravenously treated with PBS, Dex-SA, DOX plus CDDP, Dex-SA-DOX plus Dex-SA-CDDP and Dex-SA-DOX-CDDP every week for a total of 5 times at a DOX-equivalent dose of 4 mg kg^{-1} and their survivals were monitored (Fig. 5A). As shown in Fig. 5B, all the chemotherapeutic agents treated groups prolonged the survival time compared with the PBS and Dex-SA groups. After 34 weeks, the mice that received Dex-SA-DOX-CDDP, Dex-SA-DOX plus Dex-SA-CDDP and DOX plus CDDP had a survival rate of 24, 16 and 16%, while only 4 and 8% of the Dex-SA- and PBS-treated mice survived, respectively. Further observation indicated that the mice treated with Dex-SA-DOX-CDDP showed mean survival time of 29.1 weeks, whereas the mice treated with PBS only had the average survival time of 25.6 weeks (**$p < 0.01$), implying the Dex-SA-DOX-

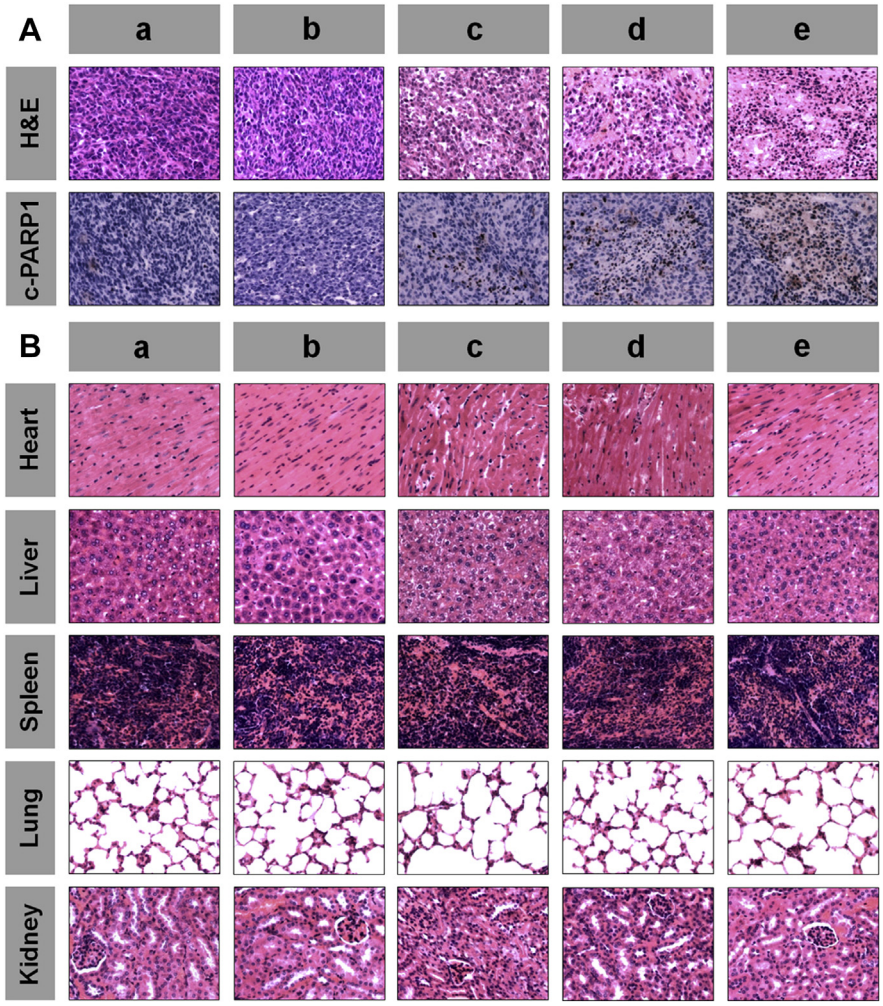

Fig. 4. Histological observation of CT26 xenograft tumors and major organs after the treatment of (a) PBS, (b) Dex-SA, (c) DOX plus CDDP, (d) Dex-SA-DOX plus Dex-SA-CDDP and (e) Dex-SA-DOX-CDDP. (A) H&E and immunohistochemical analyses of CT26 tumor sections (16 days after the first treatment). Nuclei were stained bluish violet, whereas extracellular matrix and cytoplasm were stained pink in H&E staining. Brown and blue stains indicated cleaved PARP1 and nuclei, respectively, in immunohistochemical assay. (B) Histologic assessments of major organs with H&E staining in mice. The organs were harvested from CT26 tumor-bearing mice at day 16. (For interpretation of the references to colour in this figure legend, the reader is referred to the web version of this article.)

CDDP nanoparticles exerted excellent therapeutic activity in autochthonous tumor model.

Histological analysis of colon tissues further confirmed the effectiveness of Dex-SA-DOX-CDDP in colon cancer treatment (Fig. 5C). Colon sections of PBS and Dex-SA treated mice showed adenocarcinoma with papillary pattern and dysplastic zone. Whereas, the pathological tumorigenic changes in colon tissues were inhibited in various degree by the chemotherapeutic agents treated groups. Especially, the colon sections of the Dex-SA-DOX-CDDP treated group were visually not significantly different from those of healthy mice, further demonstrating that the Dex-SA-DOX-CDDP nanoparticles could inhibit the growth of colon tumors and be expected to have a high therapeutic effect on human colorectal cancer.

3.4. Antitumor effect in orthotopic mammary tumor metastasis model

Breast cancer is currently the second leading cause of cancer-related deaths among women, surpassed only by lung cancer [48]. Notably, the 5 year survival rate of breast cancer patients sharply decreases from 98% to 23% owing to distant metastases [49]. Therefore, despite many advances in its diagnosis and treatment, it is essential to design nanotechnology-based agents that can successfully target and treat metastatic breast cancer [50]. Targeting a metastatic lesion within a large population of normal cells remains a significant challenge. In addition to reducing the toxicity and altering biodistribution *via* EPR effect, further increasing the tumor accumulation of anticancer drugs *via* active targeting ligands also plays an important role in cancer therapy [49]. Recent findings demonstrated that the tumor homing and penetrating peptide iRGD increased vascular and tissue permeability and co-administration of iRGD was more effective in delivering therapeutic agents into tumor parenchyma than conjugation [25]. Enhanced antitumor effect of free DOX co-injected with iRGD was observed in an orthotopic 4T1 mouse breast cancer model [25]. Our previous study also proved that the combination of CDDP-loaded poly(ethylene glycol)-*b*-poly(L-glutamic acid) nanoparticles and iRGD could efficiently reduce the toxicity and increase the accumulation of CDDP in subcutaneous A549 xenograft model [26].

Inspired by the excellent tumor treatment efficacy of Dex-SA-DOX-CDDP in subcutaneous colorectal carcinoma, primary colorectal carcinoma models, we then further evaluated the

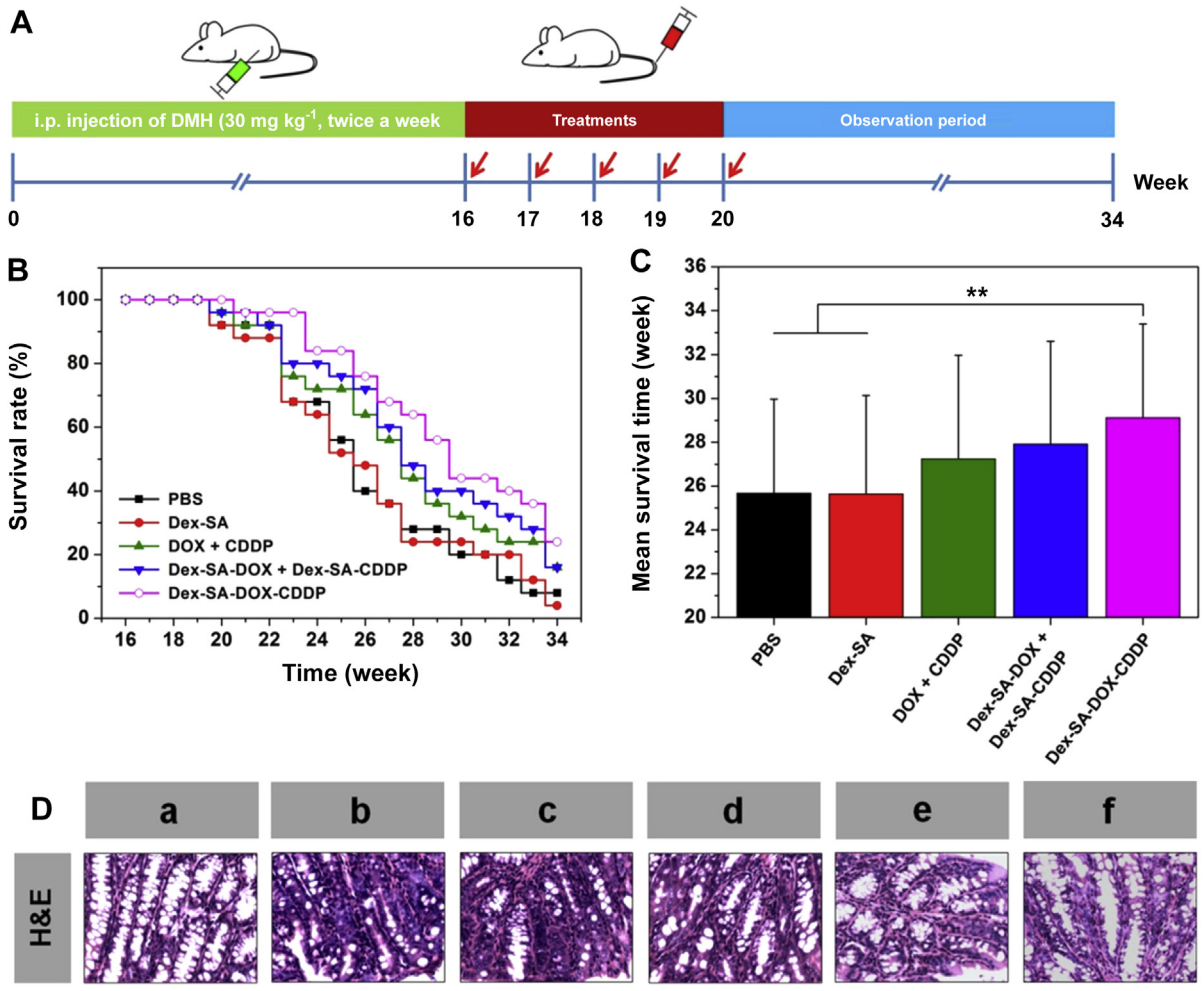

Fig. 5. Therapeutic monitoring of DMH-induced autochthonous colorectal carcinoma. Data were presented as means ± standard deviation ($n = 25$). (A) Experimental schedule for tumor induction and drug treatments. (B and C) Survival curves and mean survival time for primary-colorectal-carcinoma-bearing mice with indicated treatments. (D) Representative H&E sections of the colon tissues after the treatment of (b) PBS, (c) Dex-SA, (d) DOX plus CDDP, (e) Dex-SA-DOX plus Dex-SA-CDDP and (f) Dex-SA-DOX-CDDP, with (a) colon tissue from normal mouse as the control.

antitumor and antimetastasis activity of Dex-SA-DOX-CDDP against the orthotopic mammary tumor metastasis model. Moreover, iRGD was co-administrated to further facilitate nanoparticles extravasation from the tumor vessels and penetration into the tumor. Fig. 6A shows the tumor growth curves after intravenous injections of PBS, Dex-SA, iRGD, DOX plus CDDP, iRGD plus DOX plus CDDP, Dex-SA-DOX-CDDP and iRGD plus Dex-SA-DOX-CDDP. The tumor growth rates of mice treated with PBS, Dex-SA and iRGD were similar, indicating that Dex-SA or iRGD alone had no effect on tumor growth. In contrast, the groups injected with the DOX plus CDDP or Dex-SA-DOX-CDDP greatly delayed and inhibited tumor growth. After 20 days, the tumor volumes of mice treated with DOX plus CDDP and Dex-SA-DOX-CDDP were 770 and 425 mm^3 ($^{***}p < 0.001$, compared with PBS, Dex-SA and iRGD groups), respectively. The enhanced tumor inhibition of the Dex-SA-DOX-CDDP may be mainly due to the prolonged blood circulation and sustained drug release *in vivo* in the tumor tissue after particle accumulation *via* the EPR effect [51]. Remarkably, co-administration of iRGD would further enhance their antitumor efficacy, resulting in smaller tumor volumes of 590 and 295 mm^3 ($^{*}p < 0.05$, compared with the treatments without iRGD) for DOX plus CDDP and Dex-SA-DOX-CDDP, respectively. The combination of iRGD with Dex-SA-DOX-CDDPnanomedicine could effectively block breast cancer growth, which was believed to be benefited from the EPR-mediated tumor localization and iRGD-facilitated extravasation and tumor penetration [25,27]. Otherwise, the body weights of all the mice gradually increased except the free drugs combination treated groups throughout the experiments (Fig. 6B, $^{**}p < 0.01$, compared with all the other groups), indicating that the Dex-SA-DOX-CDDP nanoparticles treated groups did not cause severe systematic side effects, whereas the small molecule drugs could lead to significant systemic toxicity in mice.

Tumor weight was measured at the termination of the experiment and the inhibition ratios were calculated (Fig. 6C and D). The results also demonstrated that the combination of iRGD and Dex-SA-DOX-CDDP nanoparticles inhibited primary tumor growth most efficiently (83.3%), followed by Dex-SA-DOX-CDDP (72.9%), iRGD plus DOX plus CDDP (62.7%) and DOX plus CDDP (50.3%). The tumor inhibition ratios calculated by tumor weights were in good consistent with the results from tumor volume measurements.

The histologic images shown in Fig. 6E indicated that the tumors treated with iRGD plus Dex-SA-DOX-CDDP had greatly decreased cell proliferation. Their cell proliferation was significantly lower than those treated with only iRGD or with Dex-SA-DOX-CDDP, suggesting that the combination of iRGD with Dex-SA-DOX-CDDP nanoparticles could significantly reduce the number of proliferating cells within tumors. The immunohistochemical analysis also revealed that the tumors treated with iRGD plus Dex-SA-DOX-

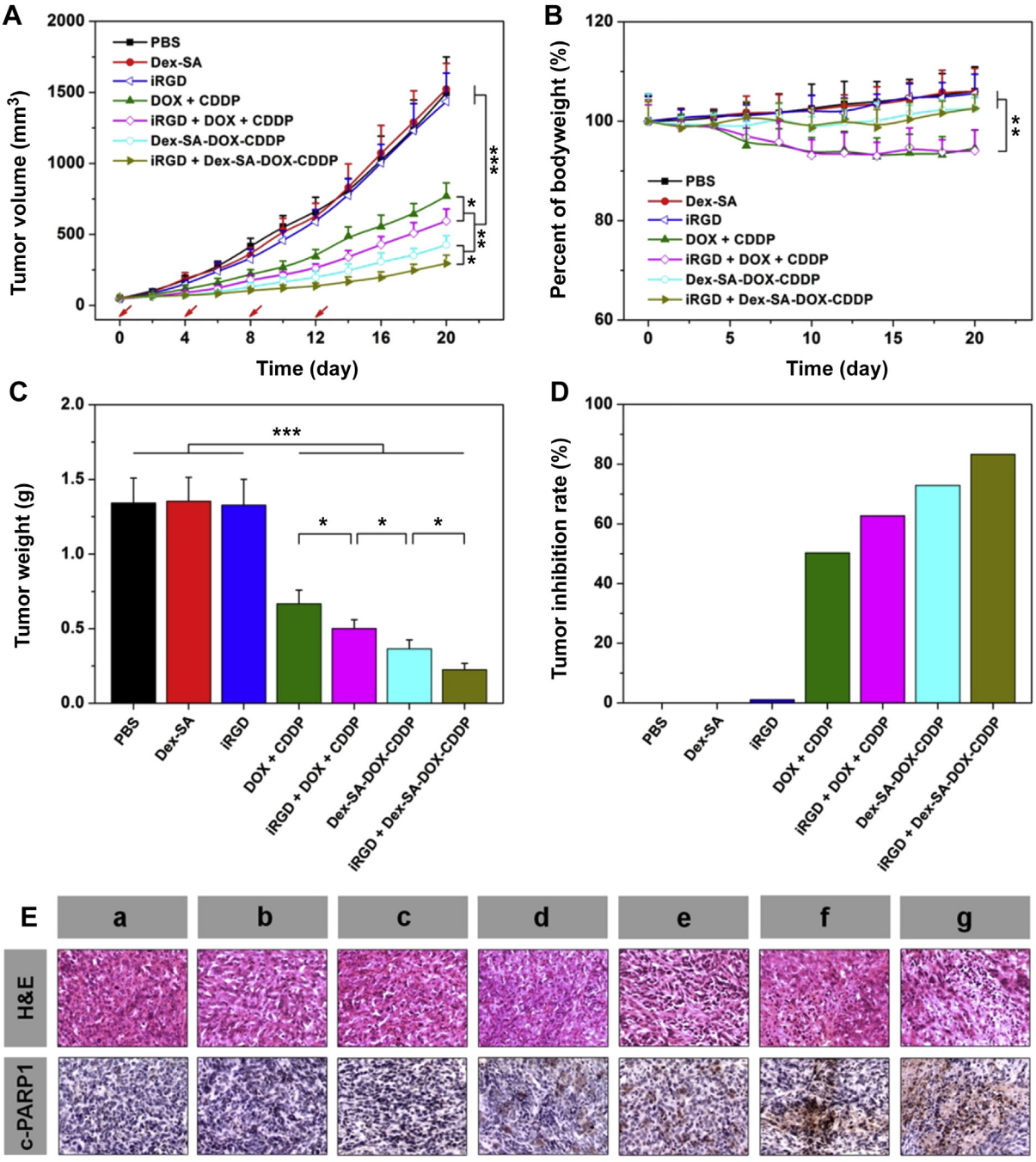

Fig. 6. *In vivo* therapeutic effects of different treatments in 4T1 orthotopic mammary tumor metastasis model. (A) The tumor volumes of mice as a function of time. Data were presented as means ± standard deviation ($n = 6$). The arrows represented the day on which the intravenous tail vein injection was performed. (B) Body weights of the mice over the experimental period. (C) The tumor weight of each group at the end of the experiment. (D) Tumor inhibition rates of various formulations. (E) H&E and immunohistochemical analyses of 4T1 tumor sections after the treatment of (a) PBS, (b) Dex-SA, (c) iRGD, (d) DOX plus CDDP, (e) iRGD plus DOX plus CDDP, (f) Dex-SA-DOX-CDDP and (g) iRGD plus Dex-SA-DOX-CDDP. Nuclei were stained bluish violet, whereas extracellular matrix and cytoplasm were stained pink in H&E staining. Brown and blue stains indicated cleaved PARP1 and nuclei, respectively, in immunohistochemical assay. (For interpretation of the references to colour in this figure legend, the reader is referred to the web version of this article.)

CDDP underwent significant apoptosis, leading to continued and effective inhibition of tumor growth.

Tumor metastasis is one of the most vital causes resulting in the high mortality of cancer patients [7,52]. Particularly, fatal pulmonary metastasis, the spread of cancer cells into the lung, usually results in a quick death of cancer patients [53]. In our mammary tumor metastasis model, a large number of metastatic sites in the lungs of the untreated mice were observed at day 20 (Fig. 7A). Abundant tumor nodules were also observed in mice treated with Dex-SA or DOX plus CDDP, indicating that the treatment with free drugs alone was not sufficient to prevent cancer metastasis. In contrast, compared to iRGD plus DOX plus CDDP, or Dex-SA-DOX-CDDP treated groups, only minimal signal of pulmonary metastasis was seen from mice treated with iRGD plus Dex-SA-DOX-CDDP. All the experimental data showed that iRGD plus Dex-SA-DOX-CDDP possessed a strong ability to overcome lung tumor metastases, besides effectively inhibiting primary tumor growth. To further assess the antimetastatic activity of our

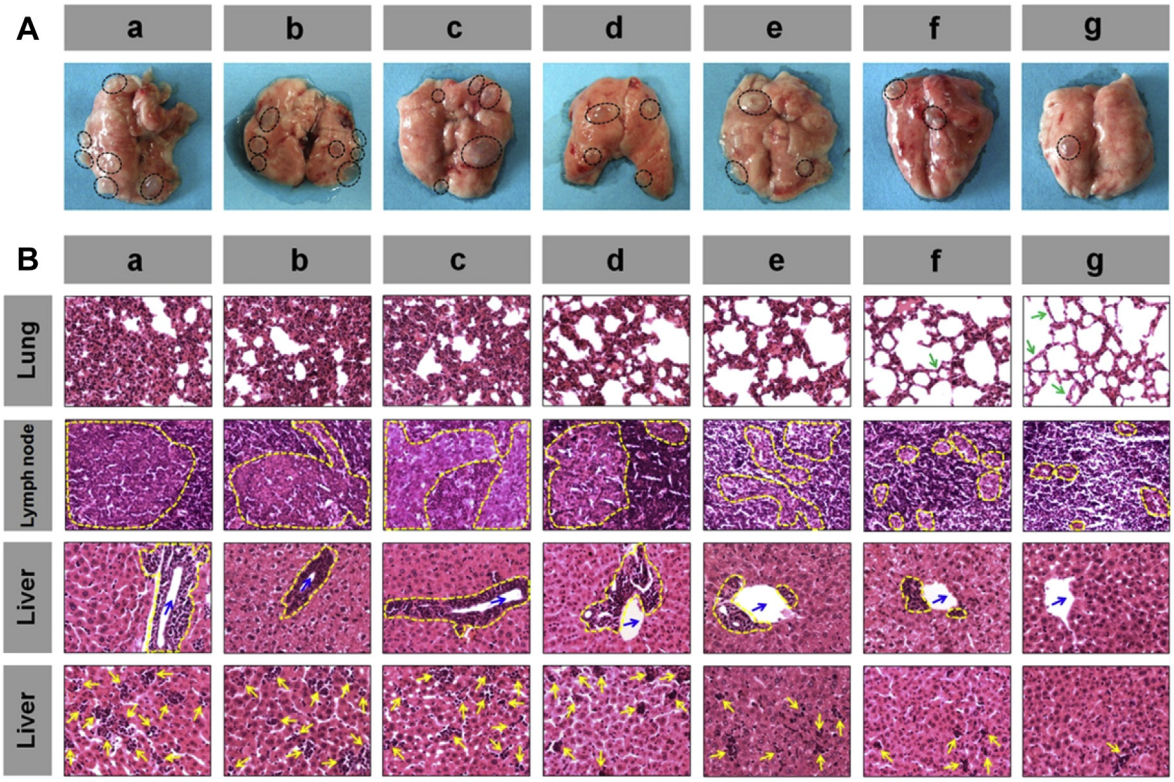

Fig. 7. Antimetastatic activities of (a) PBS, (b) Dex-SA, (c) iRGD, (d) DOX plus CDDP, (e) iRGD plus DOX plus CDDP, (f) Dex-SA-DOX-CDDP and (g) iRGD plus Dex-SA-DOX-CDDP in a metastatic mammary tumor model. (A) Representative lung images of tumor-bearing mice treated with different formulations. The dashed black lines delineated the tumor edge. (B) Representative H&E sections of the lung, lymph node and liver after metastasis from control and drug-treated mice. The dashed yellow lines and yellow arrows indicated the metastasis foci. The green arrows pointed to the normal lung tissue. The blue arrows indicated the hepatic veins. (For interpretation of the references to colour in this figure legend, the reader is referred to the web version of this article.)

developed drug delivery system, the representative sections of several susceptible organs including the lung, lymph node, and liver from mice receiving various drug formulations were harvested and stained by H&E. As shown in Fig. 7B, the mice treated with iRGD plus Dex-SA-DOX-CDDP showed only minimal levels of metastasis in these organs, and the architectures were left largely intact. Whereas, the mice treated with PBS, Dex-SA, iRGD or DOX plus CDDP had massive tumor metastasis, with the majority of the organic tissues occupied by tumor cells. It is worthy of note that mice administrated with PBS, Dex-SA or iRGD showed not only the diffuse metastatic lesion consisted of neoplastic cells around the hepatic vessels, but also the multifocal metastasis in the whole livers. Although iRGD plus DOX plus CDDP and Dex-SA-DOX-CDDP treatment decreased the tumor metastasis to some extent, iRGD plus Dex-SA-DOX-CDDP treatment was the most effective to inhibit tumor metastasis. All the experimental data have clearly evidenced that the iRGD plus Dex-SA-DOX-CDDP treatment afforded significant advantages in inhibiting breast tumor metastasis, which was the important advance in clinical cancer therapy.

4. Conclusions

Dex-SA-DOX-CDDP nanoparticles as the combination of anticanceragent efficiently inhibit cancer tissue growth *in vivo* of subcutaneously-implanted colorectal carcinoma, primary colorectal carcinoma and orthotopic mammary tumor metastasis. With specific biochemical properties of Dex-SA-DOX-CDDP in prolonged blood circulation, enhanced drug accumulation and facilitated intracellular release in the tumor cells, the CL-Nanoparticles offer an efficient antitumor agent to treat colorectal primary cancer and breast metastasis tumors, respectively. *In vivo* data suggested that Dex-SA-DOX-CDDP nanoparticles were able to inhibit the pathological tumorigenic changes in colon tissues and significantly extend the lifespan of colon cancer bearing mice. In addition, by co-administration of iRGD, Dex-SA-DOX-CDDP effectively block primary tumor growth, and further prevent the metastasis of murine mammary carcinoma. With the simple and controllable preparation process, reliable safety and flexible dosing regimen, the Dex-SA-DOX-CDDP nanoparticles hold great potential for achieving an optimal therapeutic effect in the clinical cancer treatment. Future directions will be site of action with anticancer drug delivery on cancer stem cells *via* this controlled release of nanoparticle system.

Acknowledgment

This research was financially supported by National Natural Science Foundation of China (Projects 51173184, 51373168, 21104076, 51233004, 51390484 and 51321062), Ministry of Science and Technology of China (International Cooperation and Communication Program 2011DFR51090) and Program of Scientific Development of Jilin Province (20130727050YY and 20130206066GX).

Appendix A. Supplementary data

Supplementary data related to this article can be found at http://dx.doi.org/10.1016/j.biomaterials.2015.02.002.

References

[1] Siegel R, Ma J, Zou Z, Jemal A. Cancer statistics. CA Cancer J Clin 2014;2014(64):9–29.
[2] Tenbaum SP, Ordonez-Moran P, Puig I, Chicote I, Arques O, Landolfi S, et al. beta-catenin confers resistance to PI3K and AKT inhibitors and subverts FOXO3a to promote metastasis in colon cancer. Nat Med 2012;18:892–901.
[3] Shen J, Sun H, Xu P, Yin Q, Zhang Z, Wang S, et al. Simultaneous inhibition of metastasis and growth of breast cancer by co-delivery of twist shRNA and paclitaxel using pluronic P85-PEI/TPGS complex nanoparticles. Biomaterials 2013;34:1581–90.
[4] Choi KY, Jeon EJ, Yoon HY, Lee BS, Na JH, Min KH, et al. Theranostic nanoparticles based on PEGylated hyaluronic acid for the diagnosis, therapy and monitoring of colon cancer. Biomaterials 2012;33:6186–93.
[5] O'Brien CA, Pollett A, Gallinger S, Dick JE. A human colon cancer cell capable of initiating tumour growth in immunodeficient mice. Nature 2007;445:106–10.
[6] Seib FP, Kaplan DL. Doxorubicin-loaded silk films: drug-silk interactions and in vivo performance in human orthotopic breast cancer. Biomaterials 2012;33:8442–50.
[7] He Q, Shi J. MSN anti-cancer nanomedicines: chemotherapy enhancement, overcoming of drug resistance, and metastasis inhibition. Adv Mater 2014;26:391–411.
[8] Chaffer CL, Weinberg RA. A perspective on cancer cell metastasis. Science 2011;331:1559–64.
[9] Peer D, Karp JM, Hong S, Farokhzad OC, Margalit R, Langer R. Nanocarriers as an emerging platform for cancer therapy. Nat Nanotechnol 2007;2:751–60.
[10] Cabral H, Matsumoto Y, Mizuno K, Chen Q, Murakami M, Kimura M, et al. Accumulation of sub-100 nm polymeric micelles in poorly permeable tumours depends on size. Nat Nanotechnol 2011;6:815–23.
[11] Taurin S, Nehoff H, Greish K. Anticancer nanomedicine and tumor vascular permeability; where is the missing link? J Control Release 2012;164:265–75.
[12] Sun TM, Wang YC, Wang F, Du JZ, Mao CQ, Sun CY, et al. Cancer stem cell therapy using doxorubicin conjugated to gold nanoparticles via hydrazone bonds. Biomaterials 2014;35:836–45.
[13] Dinndorf PA, Gootenberg J, Cohen MH, Keegan P, Pazdur R. FDA drug approval summary: pegaspargase (Oncaspar (R)) for the first-line treatment of children with acute lymphoblastic leukemia (ALL). Oncologist 2007;12:991–8.
[14] Deng C, Jiang Y, Cheng R, Meng F, Zhong Z. Biodegradable polymeric micelles for targeted and controlled anticancer drug delivery: promises, progress and prospects. Nano Today 2012;7:467–80.
[15] Morton CL, Houghton PJ. Establishment of human tumor xenografts in immunodeficient mice. Nat Protoc 2007;2:247–50.
[16] Jenkins DE, Oei Y, Hornig YS, Yu SF, Dusich J, Purchio T, et al. Bioluminescent imaging (BLI) to improve and refine traditional murine models of tumor growth and metastasis. Clin Exp 2003;20:733–44.
[17] Ruggeri BA, Camp F, Miknyoczki S. Animal models of disease: pre-clinical animal models of cancer and their applications and utility in drug discovery. Biochem Pharmacol 2014;87:150–61.
[18] Kung AL. Practices and pitfalls of mouse cancer models in drug discovery. Adv Cancer Res 2007;96:191–212.
[19] Becher OJ, Holland EC. Genetically engineered models have advantages over xenografts for preclinical studies. Cancer Res 2006;66:3355–8.
[20] Takahashi M, Hori M, Mutoh M, Wakabayashi K, Nakagama H. Experimental animal models of pancreatic carcinogenesis for prevention studies and their relevance to human disease. Cancers 2011;3:582–602.
[21] Abel EL, Angel JM, Kiguchi K, DiGiovanni J. Multi-stage chemical carcinogenesis in mouse skin: fundamentals and applications. Nat Protoc 2009;4:1350–62.
[22] Smith PA, Merritt D, Barr L, Thorley-Lawson DA. An orthotopic model of metastatic nasopharyngeal carcinoma and its application in elucidating a therapeutic target that inhibits metastasis. Genes Cancer 2011;2:1023–33.
[23] Li M, Tang Z, Lv S, Song W, Hong H, Jing X, et al. Cisplatin crosslinked pH-sensitive nanoparticles for efficient delivery of doxorubicin. Biomaterials 2014;35:3851–64.
[24] Teesalu T, Sugahara KN, Kotamraju VR, Ruoslahti E. C-end rule peptides mediate neuropilin-1-dependent cell, vascular, and tissue penetration. Proc Natl Acad Sci U S A 2009;106:16157–62.
[25] Sugahara KN, Teesalu T, Karmali PP, Kotamraju VR, Agemy L, Greenwald DR, et al. Coadministration of a tumor-penetrating peptide enhances the efficacy of cancer drugs. Science 2010;328:1031–5.
[26] Song W, Li M, Tang Z, Li Q, Yang Y, Liu H, et al. Methoxypoly(ethylene glycol)-block-Poly(L-glutamic acid)-loaded cisplatin and a combination with iRGD for the treatment of non-small-cell lung cancers. Macromol Biosci 2012;12:1514–23.
[27] Gu G, Gao X, Hu Q, Kang T, Liu Z, Jiang M, et al. The influence of the penetrating peptide iRGD on the effect of paclitaxel-loaded MT1-AF7p-conjugated nanoparticles on glioma cells. Biomaterials 2013;34:5138–48.
[28] Chow EK, Ho D. Cancer nanomedicine: from drug delivery to imaging. Sci Transl Med 2013;5:216rv4.
[29] Pu YJ, Chang S, Yuan H, Wang G, He B, Gu ZW. The anti-tumor efficiency of poly(L-glutamic acid) dendrimers with polyhedral oligomeric silsesquioxane cores. Biomaterials 2013;34:3658–66.
[30] Ke XY, Lin Ng VW, Gao SJ, Tong YW, Hedrick JL, Yang YY. Co-delivery of thioridazine and doxorubicin using polymeric micelles for targeting both cancer cells and cancer stem cells. Biomaterials 2014;35:1096–108.
[31] Sengottuvelan M, Viswanathan P, Nalini N. Chemopreventive effect of trans-resveratrol-a phytoalexin against colonic aberrant crypt foci and cell proliferation in 1,2-dimethylhydrazine induced colon carcinogenesis. Carcinogenesis 2006;27:1038–46.
[32] Wang J, Sun X, Mao W, Sun W, Tang J, Sui M, et al. Tumor redox heterogeneity-responsive prodrug nanocapsules for cancer chemotherapy. Adv Mater 2013;25:3670–6.
[33] Fu C, Lin L, Shi H, Zheng D, Wang W, Gao S, et al. Hydrophobic poly (amino acid) modified PEI mediated delivery of rev-casp-3 for cancer therapy. Biomaterials 2012;33:4589–96.
[34] Li YL, Zhu L, Liu Z, Cheng R, Meng F, Cui JH, et al. Reversibly stabilized multifunctional dextran nanoparticles efficiently deliver doxorubicin into the nuclei of cancer cells. Angew Chem Int Ed 2009;48:9914–8.
[35] Ganta S, Devalapally H, Shahiwala A, Amiji M. A review of stimuli-responsive nanocarriers for drug and gene delivery. J Control Release 2008;126:187–204.
[36] Sun CY, Dou S, Du JZ, Yang XZ, Li YP, Wang J. Doxorubicin conjugate of poly(ethylene glycol)-block-polyphosphoester for cancer therapy. Adv Healthc Mater 2014;3:261–72.
[37] Wang J, Wu W, Zhang Y, Wang X, Qian H, Liu B, et al. The combined effects of size and surface chemistry on the accumulation of boronic acid-rich protein nanoparticles in tumors. Biomaterials 2014;35:866–78.
[38] Xiao K, Li Y, Luo J, Lee JS, Xiao W, Gonik AM, et al. The effect of surface charge on in vivo biodistribution of PEG-oligocholic acid based micellar nanoparticles. Biomaterials 2011;32:3435–46.
[39] Zhang LZ, Zhang YJ, Wu W, Jiang XQ. Doxorubicin-loaded boron-rich polymer nanoparticles for orthotopically implanted liver tumor treatment. Chin J Polym Sci 2013;31:778–86.
[40] Ding J, Xu W, Zhang Y, Sun D, Xiao C, Liu D, et al. Self-reinforced endocytoses of smart polypeptide nanogels for “on-demand” drug delivery. J Control Release 2013;172:444–55.
[41] Lv S, Tang Z, Li M, Lin J, Song W, Liu H, et al. Co-delivery of doxorubicin and paclitaxel by PEG-polypeptide nanovehicle for the treatment of non-small cell lung cancer. Biomaterials 2014;35:6118–29.
[42] He LZ, Huang YY, Zhu HL, Pang GH, Zheng WJ, Wong YS, et al. Cancer-targeted monodisperse mesoporous silica nanoparticles as carrier of ruthenium polypyridyl complexes to enhance theranostic effects. Adv Funct Mater 2014;24:2754–63.
[43] Zhang C, Pan D, Luo K, She W, Guo C, Yang Y, et al. Peptide dendrimer-doxorubicin conjugate-based nanoparticle as an enzyme-responsive drug delivery system for cancer therapy. Adv Healthc Mater 2014;3:1299–308.
[44] Shilpa J, Pretty MA, Anitha M, Paulose CS. Gamma aminobutyric acid B and 5-hydroxy tryptamine 2A receptors functional regulation during enhanced liver cell proliferation by GABA and 5-HT chitosan nanoparticles treatment. Eur J Pharmacol 2013;715:154–63.
[45] Sharpless NE, Depinho RA. The mighty mouse: genetically engineered mouse models in cancer drug development. Nat Rev Drug Discov 2006;5:741–54.
[46] Roscilli G, Marra E, Mori F, Di Napoli A, Mancini R, Serlupi-Crescenzi O, et al. Carnitines slow down tumor development of colon cancer in the DMH-chemical carcinogenesis mouse model. J Cell Biochem 2013;114:1665–73.
[47] Amberger H. Different autochthonous models of colorectal cancer in the rat. J Cancer Res Clin Oncol 1986;111:157–9.
[48] You JO, Guo P, Auguste DT. A drug-delivery vehicle combining the targeting and thermal ablation of HER2+ breast-cancer cells with triggered drug release. Angew Chem Int Ed 2013;52:4141–6.
[49] Peiris PM, Toy R, Doolittle E, Pansky J, Abramowski A, Tam M, et al. Imaging metastasis using an integrin-targeting chain-shaped nanoparticle. ACS Nano 2012;6:8783–95.
[50] Ma X, Zhou J, Zhang CX, Li XY, Li N, Ju RJ, et al. Modulation of drug-resistant membrane and apoptosis proteins of breast cancer stem cells by targeting berberine liposomes. Biomaterials 2013;34:4452–65.
[51] Zhang F, Braun GB, Pallaoro A, Zhang Y, Shi Y, Cui D, et al. Mesoporous multifunctional upconversion luminescent and magnetic “nanorattle” materials for targeted chemotherapy. Nano Lett 2012;12:61–7.
[52] El-Boubbou K, Zhu DC, Vasileiou C, Borhan B, Prosperi D, Li W, et al. Magnetic glyco-nanoparticles: a tool to detect, differentiate, and unlock the glyco-codes of cancer via magnetic resonance imaging. J Am Chem Soc 2010;132:4490–9.
[53] Liang C, Diao S, Wang C, Gong H, Liu T, Hong G, et al. Tumor metastasis inhibition by imaging-guided photothermal therapy with single-walled carbon nanotubes. Adv Mater 2014;26:5646–52.